Wang, T., Li, X. , Quan, Q., Harkness, P. and Deng, Z. (2024) Passive versus active control of weight-on-bit for an ultrasonic percussive drill. *IEEE/ASME Transactions on Mechatronics*, (doi: 10.1109/TMECH.2024.3360977) (Early Online Publication)

This is the author version of the work. There may be differences between this version and the published version. You are advised to consult the published version if you want to cite from it:
https://doi.org/10.1109/TMECH.2024.3360977

https://eprints.gla.ac.uk/317844/

Deposited on 31 January 2024

Enlighten – Research publications by members of the University of Glasgow

http://eprints.gla.ac.uk

Passive versus Active Control of Weight-on-Bit for an Ultrasonic Percussive Drill

Tongzhao Wang, Xuan Li, Qiquan Quan, *Senior Member, IEEE*
Patrick Harkness, and Zongquan Deng

***Abstract*—Multiple ultrasonic percussive drill cross-drilling anchoring helps to achieve long-term, secure attachment of sampling platforms in extreme environments. Ultrasonic percussive drills require less weight-on-bit (WOB) and lower power than conventional drills, making them more suitable for asteroid anchoring mission. Choosing a suitable WOB control method is one of the key factors to ensure rapid and stable drilling, but there is little research on the effect of WOB control method on ultrasonic drilling performance. To address the technical challenges of drilling, this paper investigates the effects of passive and active WOB control on ultrasonic drilling performance. Firstly, the mechanical configuration of an ultrasonic percussive drill is presented and a full-wavelength piezoelectric transducer is designed using impedance analysis (IA) and Experimental Modal Analysis (EMA). Then, passive control of WOB is implemented using suspended weights, and active control is implemented using a linear actuator. Finally, the effect of the WOB control method on drilling performance is experimentally verified on rocks with different compressive strengths. Our results show that active control is better suited to WOB variation and rock compressive strength variation. When the WOB is 5 N, the drilling rate of passive control is slightly higher than that of active control, but the difference is not significant. When the WOB is 10 N and 15 N, the drilling rate of active control surpasses that of passive control. The ultrasonic percussive drill's power consumption is less than 60 W. This paper provides a technical reference for selecting the WOB method for ultrasonic percussive drills in planetary exploration.**

***Index Terms*—Ultrasonic percussive drill, weight-on-bit, passive and active control, piezoelectric transducer, asteroid exploration.**

I. Introduction

ULTRASONIC percussive drills, with their outstanding advantages of low weight-on-bit, low power consumption, wide temperature range, no need for lubrication and simple structure, has been identified as one of the key technologies in asteroid exploration mission, which will assist sampling platforms in achieving long-term anchoring on the surface of an asteroid in the future [1]–[3].

This work was supported in part by the National Natural Science Foundation of China under Grant 51975139, Grant 51935005 and Grant 52105012, in part by the China Scholarship Council. Also, many thanks to the James Watt School of Engineering, University of Glasgow, for providing the test equipment. *(Corresponding Author: Qiquan Quan)*

Tongzhao Wang, Qiquan Quan and Zongquan Deng are with State Key Laboratory of Robotics and Systems, Harbin Institute of Technology, Harbin 150080, China (Tongzhao Wang: wangtongzh@163.com; Qiquan Quan: quanqiquan@hit.edu.cn; Zongquan Deng: dengzq@hit.edu.cn).

Xuan Li, and Patrick Harkness are with James Watt School of Engineering, University of Glasgow, Glasgow G12 8QQ, UK (Xuan Li: Xuan.Li@glasgow.ac.uk; Patrick Harkness: Patrick.Harkness@glasgow.ac.uk)

According to the specifications of the asteroid exploration mission, three ultrasonic percussive drills are arranged axially along the lander leg, and they need to penetrate the surface of the asteroid within 2 minutes. These three drills form a geometrical force closure that provides sampling platforms with an anchoring force of more than 100 N. The sampling platform has three upwards-firing thrusters which can provide the ultrasonic percussive drills with a weight-on-bit of no more than 20 N during this time. The limited drilling time and the low weight-on-bit pose a challenge to the stability of the ultrasonic drilling process.

Factors affecting the stability of ultrasonic drill include the high and low temperatures of the asteroid surface (-45 to 90°C) [4], the control method and impedance matching of the ultrasonic drive power [5], [6], the type of ultrasonic drill motion [7], [8], and the weight-on-bit control method [9]. High and low temperatures can cause changes in drilling performance by affecting the impedance characteristics of the ultrasonic drill [10]. Resonant frequency tracking and constant amplitude control of the ultrasonic drive power are crucial for maintaining the amplitude stability of the piezoelectric transducer [11], [12]. Impedance matching affects the power conversion between the ultrasonic drive power and the ultrasonic drill [13]. Types of ultrasonic drill motion include direct-drive [14], percussive [15], and rotary-percussive [16]. Direct-drive ultrasonic drilling, also known as ultrasonic-assisted drilling (UAD), generally requires a motor to maintain rotation of the bit. Rotary-percussive ultrasonic drilling using a piezoelectric transducer to generate a longitudinal and torsional composite mode can be effective, but the longitudinal and torsional composite design also increases the complexity of the structure. The ultrasonic percussive drill, with its simpler and more compact mechanical structure, is better suited to meet the challenges of sampling platforms with large time delays and high autonomy in planetary exploration.

Weight-on-bit refers to the axial force required on the drill bit during the drilling process. This force is controlled by either the drill's own weight or an external loading mechanism. Changes in the WOB affect the impedance characteristics of the piezoelectric transducer, thereby influencing the stability of the system. There is still a gap in research regarding the effect of the weight-on-bit control method on ultrasonic drilling performance.

Low WOB is one of the outstanding advantages demonstrated by Sherrit et al. using a hand-held ultrasonic drill [3]. With an ultrasonic drill placed into a plastic guide tube, where the WOB was supplied only by the weight of the

ultrasonic drill itself [17]. In the ultrasonic grinder [18], Ice-gopher [19] and Auto-gopher-I [20], developed later based on the Ultrasonic/Sonic Drilling/Coring (USDC), the WOB during drilling was provided by the weight of the ultrasonic percussive drill itself. The ultrasonic drill developed by Magna Parva and ESA also uses its own weight to provide WOB [21]. Guo et al. achieved WOB control by adding mass to the back cover of the drill [22]. All of these schemes demonstrate the outstanding advantage of low WOB for ultrasonic drills. However, on the surface of an asteroid with weak gravity, methods relying on their own weights or additional mass are not applicable. Zacny et al. used the axial feed motion of the ball screw to provide WOB for the ultrasonic auger in the design of the Auto-gopher-II [23]; and downward pressure on the bit along the axial direction of the bit to provide WOB in the design of the compacted soil auger [24]. Bao et al. used a pneumatic cylinder to provide WOB in their study of ultrasonic drilling performance at high temperatures [25]. Khmelev et al. used an electromagnetic motor to provide WOB by axial downward pressure on the drill bit [26]. Harkness et al. used only the downward pressure of the crimped pipe to provide WOB to the device in their study of a crimped ultrasonic drilling and coring device [27]. Li et al. used horizontally suspended weights to provide WOB when comparing the performance of full-wavelength and half-wavelength ultrasonic drill [28]; a linear actuator was used to provide WOB in ultrasonic-assisted drilling with active control [29]. Bai et al. used horizontally suspended weights to provide drilling force for ultrasonic drill [30]. Wang et al. used a combination of motor drive and buffer spring to provide the WOB, which has a similar effect to the scheme of horizontally suspended weights [31]. From the above summary, it can be seen that no matter which control method is used, ultrasonic drilling can be achieved by giving a smaller WOB when drilling. However, it has not yet been clarified how the ultrasonic drilling on the surface of an asteroid should choose the appropriate WOB control method.

The above WOB control methods can be summarised into three categories: mass driven (utilizing the drill's weight or hanging weights for WOB), which is passive control; control driven (employing a feed mechanism combined with active control for WOB), which is active control; and feed rate driven (using a feed mechanism for WOB). Feed rate driven is prone to drill bit jamming, which can lead to drill bit damage and sample burns. In this paper, we will compare the other two WOB control methods and investigate the effects of passive and active control on drilling performance.

In this paper, the mechanical configuration and material parameters of the ultrasonic percussive drill (UPD) are firstly given, and the full-wavelength piezoelectric transducer is designed based on IA and EMA methods. Suspended weights are used as a passive control scheme. A linear actuator combined with active control algorithm is used as active control scheme. Four analogue media, aircrete, limestone, sandstone and marble, are used to study the effects of different WOB control schemes on the drilling performance of UPD.

The remainder of this paper is organised as follows. Section II introduces the mechanical configuration of UPD and the piezoelectric transducer design method. Section III introduces the passive and active control methods of WOB. Section IV carries out the experimental verification of UPD drilling performance using the constructed test rig. Section V gives the conclusion.

II. Design of the ultrasonic percussive drill

A. Configuration of the Ultrasonic Percussive Drill

The UPD proposed in this paper consists of a full-wavelength piezoelectric transducer and a drilling tool assembly, and its mechanical configuration and assembly method are shown in Fig. 1. The piezoelectric transducer serves as the excitation unit of the UPD and comprises a back mass, a piezoelectric ceramic stack, and a stepped horn. The piezoelectric ceramic stack is driven by an ultrasonic drive power to generate a sinusoidal amplitude at a frequency of 20 kHz, and the stepped horn provides a gain of two. The longitudinal sinusoidal amplitude serves as the excitation amplitude for the drilling tool assembly. The function of the drilling tool assembly is to convert the micrometre-scale excitation amplitude into millimetre-scale longitudinal percussive motion of the drill tool. The drilling tool assembly consists of a free mass, a restoring spring and a drill tool. The free mass functions as a vibration energy conversion unit, oscillating back and forth between the stepped horn and the drill tool. It converts the ultrasonic vibrations generated by the piezoelectric transducer into high-frequency vibrations of the drill tool. A restoring spring provides the restoring force for the free mass to oscillate back and forth. Importantly, there is no mechanical connection between the free mass and the drill tool, only the restoring spring presses them together at the front of the stepped horn. The free mass exhibits chaotic motion with a frequency range of approximately 10 to 1000 Hz. This assembly of the drilling tool assembly causes the UPD to exhibit a form of motion that is a longitudinal percussive motion.

The assembly pre-tensioning torque of the piezoelectric transducer is 150 Nm. In order to ensure the consistency of the tightening torque change of the piezoelectric transducer when the surface temperature of the asteroid varies, the materials of the back mass and the stepped horn are both TC4 titanium alloy. The piezoelectric ceramics were chosen to be PZT8 ceramics polarised along the Z-axis (outer diameter 35 mm, inner diameter 16 mm, thickness 3 mm), whose piezoelectric stress matrix d, elasticity matrix E, and relative dielectric constant matrix ε are respectively

$$[d] = \begin{bmatrix} 0 & 0 & -3.9 \\ 0 & 0 & -3.9 \\ 0 & 0 & 13.9 \\ 0 & 10.3 & 0 \\ 10.3 & 0 & 0 \end{bmatrix} \times 10^{-11}\ \mathrm{C/m^2}$$

$$[E] = \begin{bmatrix} 14.7 & 8.1 & 8.1 & 0 & 0 & 0 \\ 8.1 & 14.7 & 8.1 & 0 & 0 & 0 \\ 8.1 & 8.1 & 13.2 & 0 & 0 & 0 \\ 0 & 0 & 0 & 3.3 & 0 & 0 \\ 0 & 0 & 0 & 0 & 3.1 & 0 \\ 0 & 0 & 0 & 0 & 0 & 3.1 \end{bmatrix} \times 10^{10}\ \mathrm{N/m^2}$$

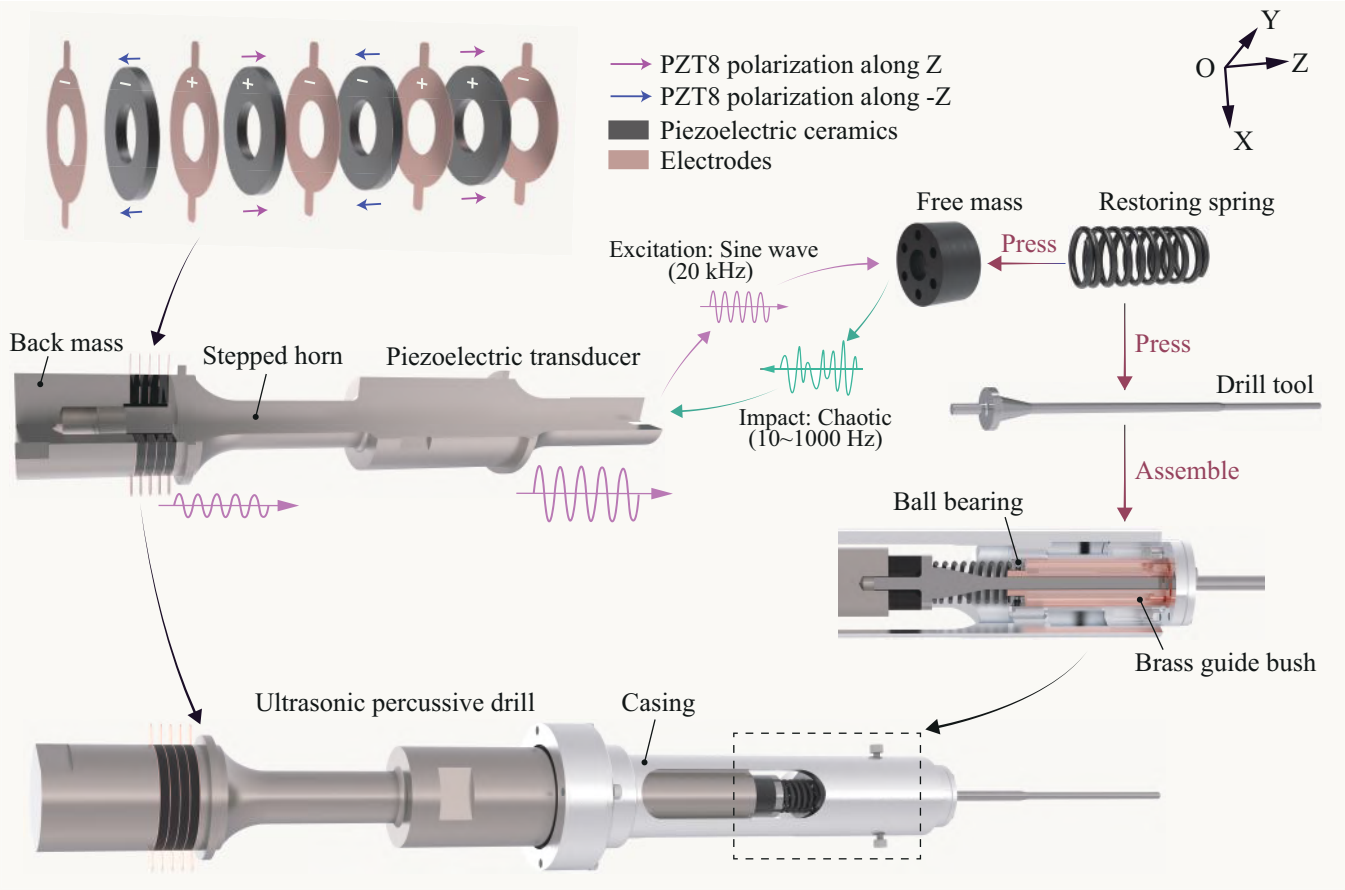

Fig. 1. Mechanical configuration and assembly of ultrasonic percussive drill.

$$[\varepsilon] = \begin{bmatrix} 901 & 0 & 0 \\ 0 & 904 & 0 \\ 0 & 0 & 561 \end{bmatrix}$$

The free mass needs high hardness and toughness to withstand repeated high-frequency percussion. After experimental verification, spring steel 65Si2Mn is selected as the material for the free mass, and the hardness reaches 45∼50 HRC after heat treatment. To ensure that the coefficient of strength of the restoring spring remains consistent in both high and low temperature environments, GH4169 is selected as the material for the restoring spring. The restoring spring pre-pressure is between 15 N and 20 N. The drill tool is made of tungsten steel with a grade of YG 10. Tungsten steel drill tools can penetrate basalt with compressive strengths exceeding 200 MPa, enhancing their suitability for drilling into rocks with unknown compressive strengths on the surface of the asteroid. We have carried out a detailed theoretical analysis of parameter determination of the drilling tool assembly in the literature [32]. The dimensions of the individual parts of the UPD are provided in Table I.

TABLE I
DIMENSIONAL PARAMETERS OF EACH PART OF UPD

Parameter	Units	Value
Back mass diameter	mm	35
Back mass length	mm	37
Stepped horn large diameter	mm	35
Primary stepped horn small diameter	mm	18
Secondary stepped horn small diameter	mm	20
Stepped horn length	mm	205
Free mass outer diameter	mm	16
Free mass inner diameter	mm	6
Free mass thickness	mm	9
Restoring spring parameters	mm	$\phi 1.2 \times 12.4 \times 40$
Drill tool diameter	mm	4
Total length of drill tool	mm	192
Rear length of drill tool	mm	15

B. Electrical Impedance Analysis (IA)

The piezoelectric transducer excites the drilling tool assembly to produce longitudinal impact vibration, and its design performance is a prerequisite for the stable operation of UPD. Methods for evaluating the design performance of piezoelectric transducers include impedance characterisation, modal analysis and amplitude testing. The theoretical design frequency of the piezoelectric transducer is 20 kHz. After assembling the piezoelectric transducer, the impedance characteristics of the piezoelectric transducer were tested using an impedance analyser (4294A, Agilent, Santa Clara, CA, USA).

The piezoelectric transducer was placed horizontally on the optical platform and the test results are shown in Fig. 2. The measured series resonant frequency is 19.987 kHz and the

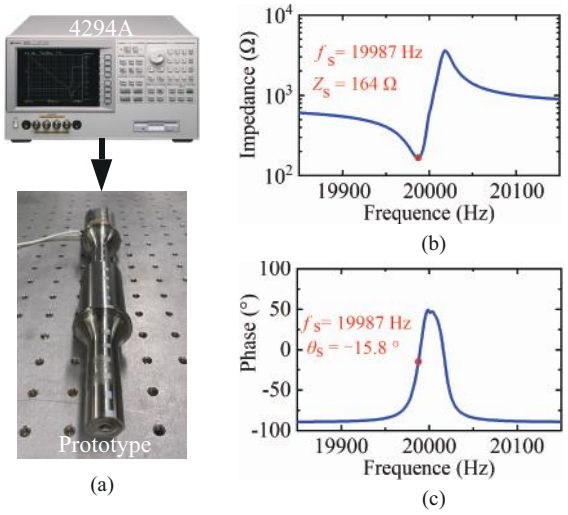

Fig. 2. Impedance testing of the piezoelectric transducer. (a) Impedance analyser and prototype piezoelectric transducer. (b) Impedance curve. (c) Phase curve.

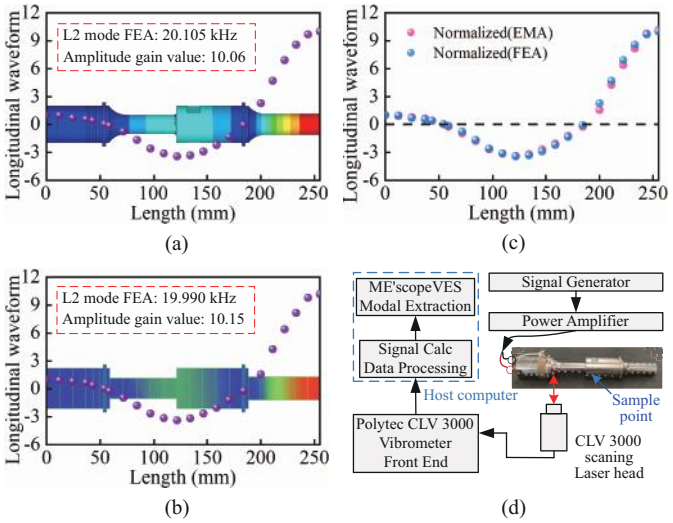

Fig. 3. Simulated and measured vibration mode shapes and longitudinal waveforms of the piezoelectric transducer: (a) FEA mode shape. (b) EMA mode shape. (c) Comparison of FEA and EMA Modal Shapes. (d) Diagram of EMA excitation and measurement systems.

series resonant impedance is 164 Ω. The impedance analyser can simultaneously obtain the equivalent electrical parameters of the piezoelectric transducer. The equivalent electrical parameters are used to further calculate the electrical coupling coefficient k_c and mechanical quality factor Q_m.

$$k_c = \sqrt{\frac{C_1}{C_1 + C_0}} \tag{1}$$

$$Q_m = \frac{1}{R_1}\sqrt{\frac{L_1}{C_1}} \tag{2}$$

where L_1 represents the dynamic inductance of the piezoelectric transducer, C_1 represents the dynamic capacitance, R_1 represents the dynamic resistance, and C_0 represents the static capacitance. After calculation, k_c and Q_m are values of 0.066 and 7589 respectively.

C. Experimental Modal Analysis (EMA)

Experimental modal analysis is used to verify the modal parameters of the designed piezoelectric transducer including frequency, damping and mode shape. The experimental modal analysis consists of two parts: calculating the frequency response function and extracting the modal parameters. The excitation signal required for calculating the frequency response function is provided by a signal generator and a power amplifier. The signal generator produces a random white noise voltage signal with an RMS value of 1 V and a frequency range of 0 to 80 kHz. The random white noise voltage signal is amplified by a power amplifier to an RMS value of 10 V, and is then fed into the positive and negative electrodes of the piezoelectric transducer. The response signal was obtained by 3D laser Doppler vibrometer testing three orthogonal components of the vibrational velocity at sampling points on the surface of the piezoelectric transducer. Four columns of sampling points in the circumferential direction on the surface of the piezoelectric transducer. There are 23 sampling points in each column, and the axial spacing of the sampling points is evenly distributed. The position of the laser vibrometer was moved during the test to obtain acquisition of the vibration response at different sampling points. In order to prevent temperature rise from affecting the performance of the piezoelectric transducer, the sampling interval between two sampling points was 5 minutes. After obtaining the vibration response data of all sampling points, the data are imported into the data processing software of the host computer, which can obtain the frequency response function of the piezoelectric transducer. Subsequently, the amplitude and phase of the frequency response function are extracted from the frequency response function using the curve fitting method. Finally, the modal parameters (frequency, damping and mode shape) of the piezoelectric transducer and the mode shape animation diagram are obtained using the modal analysis software of the host computer.

The signal generator is Quattro, Data Physics, Santa Clara, CA, USA. The power amplifier is RMX 4050HD, QSC Audio Products, Costa Mesa, CA, USA. The model of the 3-D laser Doppler vibrometer is CLV3000, Polytec, Waldbronn, Germany. The model of the data processing software is SignalCalc, Data Physics, Santa Clara, CA, USA. The model of the modal extraction software is ME'scopeVES, Vibrant Technology Inc, Centennial, CO, USA.

Fig. 3 shows the mode shape of the piezoelectric transducer obtained from FEM and EMA and the longitudinal vibration velocity at each test point, respectively. The longitudinal vibration velocities at each test point have been normalised in the figure. As can be seen from the figure, the longitudinal oscillation wavelength of the piezoelectric transducer is the full wavelength, and the maximum amplitude occurs at the front face of the stepped horn. The piezoelectric transducer has two zero amplitude nodes distributed on the two flanges. The frequency of the FEM design is 20.103 kHz and the frequency of the EMA test is 19.990 kHz, and the frequency difference between the two is 113 Hz. Comparing the front face of

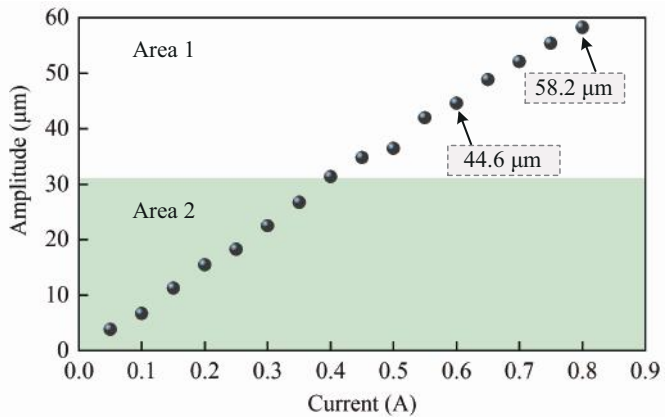

Fig. 4. Relationship between current and amplitude of the piezoelectric transducer.

the stepped horn amplitude and the back mass amplitude, it can be concluded that the amplitude gains obtained by the FEM and the EMA are 10.06 and 10.15, respectively. Besides, the damping value of the piezoelectric transducer, tested through EMA, is 0.0088%. The resulting experimental modal test verifies the feasibility of using ANSYS to design the piezoelectric transducer, and the modal parameters of the two are basically the same.

D. Amplitude of the Piezoelectric Transducer

The amplitude of the front face of the piezoelectric transducer was determined through 1D laser Doppler vibrometer testing. To drive the piezoelectric transducer, we used a signal generator (Agilent 33210A, Keysight, Santa Clara, CA, USA) and a power amplifier (HFVA-62, Nanjing Foneng Technology Industry Ltd., Nanjing, China). The signal generator supplied a sinusoidal AC signal to the power amplifier, which operated in a constant current mode.

The relationship between the current value and the amplitude of the piezoelectric transducer was initially investigated by testing the amplitudes corresponding to various current values. Due to the limited power of the power amplifier, the maximum output current set for testing was 0.8 A. A total of 16 sets of tests were conducted, with the peak current incrementing from 0.05 to 0.8 A in increments of 0.05 A. The results of these tests are depicted in Fig. 4, demonstrating a linear increase in the amplitude of the piezoelectric transducer with the rising current.

Subsequently, the piezoelectric transducer was assembled onto the UPD, and 16 sets of current values were employed to sequentially activate the UPD for rock drilling. Based on the vibration state of the UPD, it was observed that when the current values fell within Area 2 (current less than 0.4 A), the UPD remained unable to vibrate due to the low amplitude. Conversely, when the current values were within Area 1 (current greater than 0.4 A), the UPD vibrated and successfully drilled into the rock.

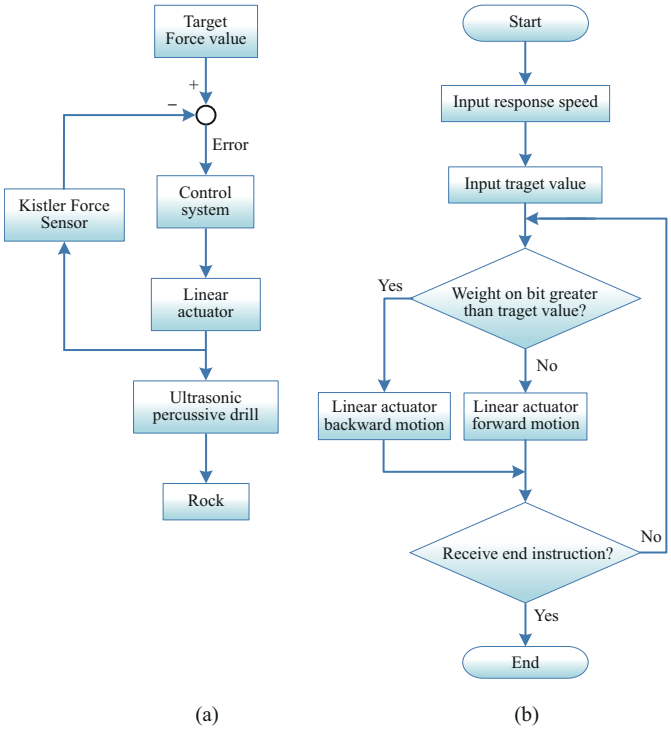

Fig. 5. Design of the active control programme. (a) Flowchart for WOB active control. (b) Flowchart for linear actuator control algorithm.

III. Control Scheme of the WOB

A. Passive control

Passive control of the WOB was achieved by means of hanging weights. Weights of 500 g, 1000 g and 1500 g were selected as three sets of test parameters. Passive control of the WOB was implemented by simply adjusting the mass of the weights before the commencement of each test set. The drilling depth of the UPD was continuously monitored in real-time using a position sensor (PS C15M 200, Position Sensors Ltd., Verwood, UK). Suspended weights are straightforward to operate and are ideal for swiftly assessing the drilling performance of ultrasonic drills. They have been widely utilized in various literature studies.

B. Active control

Active control of the WOB was achieved by regulating the feed movement of the linear actuator (GLA 750 12V DC, Gimson robotics, Bristol, UK). The compression force between the linear actuator and the UPD is the WOB, which was captured in real time by the force sensor (Kistler 9321B, Kistler, Switzerland) during the drilling process. The difference between the actual WOB value and the target value was used as input to the linear actuator control system. The control system adjusted the movement of the linear actuator to maintain the WOB value at the desired target level. The real-time motion trajectory of the linear actuator was used to track the drilling depth of the UPD. The active control flow of WOB is shown in Fig. 5(a).

The control algorithm for the linear actuator was developed using the Arduino IDE platform. The flow chart of the control

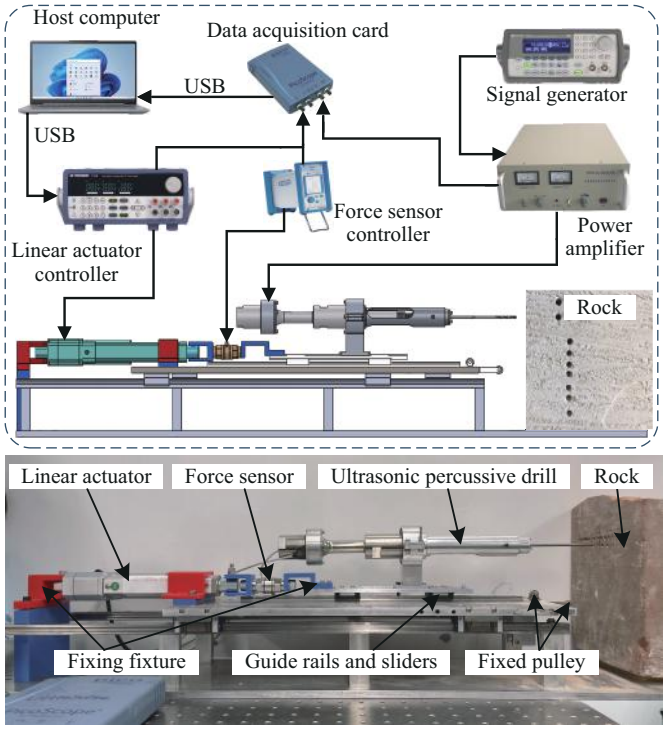

Fig. 6. Test rig.

TABLE II
MATERIAL PARAMETERS OF ROCK FOR DRILLING TESTS [29]

Material	ρ[kg/m^3]	Porosity[%]	Hardness[Mohs]	UCS[MPa]
Aircrete	350	85	—	3.5
Limestone	2550	5.3	3.4	30
Sandstone	2600	—	—	40
Marble	2750	0.49	4	100

algorithm is shown in Fig. 5(b). The target values of WOB are 5 N, 10 N and 15 N, respectively. When the linear actuator is activated, both the UPD and the linear actuator move in unison. The force sensor continuously monitors the WOB, and if it detects that the WOB exceeds the target value, the linear actuator moves backward alongside the UPD. Conversely, if the WOB falls below the target value, the linear actuator moves forward together with the UPD. Once the UPD reaches the predetermined drilling time, the linear actuator receives a stop command, and the drilling process concludes.

IV. EXPERIMENT RESULTS

A. Test rig

The test rig for the UPD is shown in Fig. 6, equipped with both passive and active control functions for WOB. The UPD is driven by a signal generator (Agilent 33210A) and a power amplifier (HFVA-62), securely mounted on two sliders along a horizontal rail. The UPD consistently operates at a frequency of 20.190 kHz, whether using passive or active control methods. When drilling rock with a fixed frequency excitation UPD, the voltage and current signals at both ends of the UPD were collected and found to be stable within a certain range. At the same time, we drive the UPD with a lower voltage value resulting in less temperature increase in 1 minute. Therefore, we set the excitation frequency of UPD to a fixed frequency.

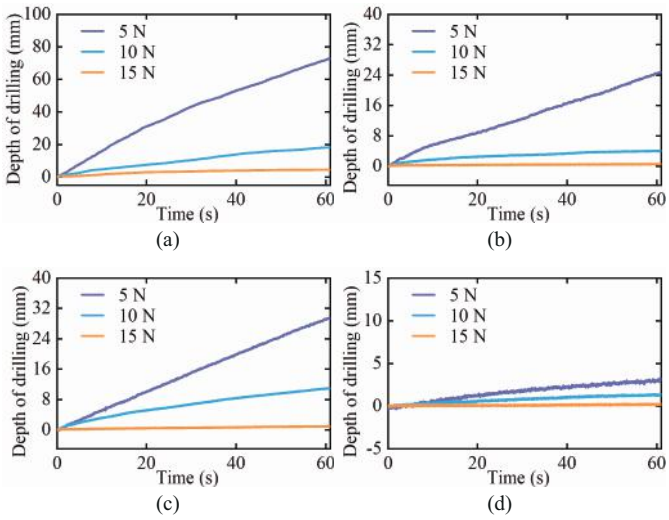

Fig. 7. Drilling depth with WOB passive control. (a) Aircrete. (b) Limestone. (c) Sandstone. (d) Marble.

During passive control testing of the WOB, weights are suspended using Kevlar rope. The Kevlar rope is wound around two fixed pulleys and attached to the bracket of the UPD. For active control testing of the WOB, the linear actuator is positioned axially to the drill tool, and a force sensor is placed between the linear actuator and the UPD. Rigid brackets connect the ends of the force sensor. The control system for the linear actuator motion includes an Arduino board and a dual-bridge motor controller. The controller for the force sensor is model Kistler 5015. The trajectory of the linear actuator and the WOB values from the force sensor are captured using the data acquisition card Picoscope 4424 and then transferred to the host computer. Parameter settings, data storage, data processing, and result visualization are carried out on the host computer. The rocks are securely fixed on the test rig, and their material properties are detailed in Table II.

B. Drilling Tests of Passive Control

Firstly, we investigated the drilling performance of the UPD under passive WOB control. The duration of a single drilling session was set to 1 minute. The output current of the power amplifier was maintained at 0.6 A, corresponding to a piezoelectric transducer amplitude of 44.6 μm. To minimize the impact of UPD's temperature rise on drilling performance, a 30-minute time interval separated each set of tests.

The test results are shown in Fig. 7. The UPD drilled stably in all four types of rock and at different WOB. The smaller the WOB, the faster the drilling rate of UPD. When the WOB was set at 5 N, the drilling depths achieved on aircrete, limestone, sandstone, and marble were 73.2 mm, 24.8 mm, 29.5 mm, and 3.2 mm, respectively. However, as the WOB was increased to 10 N and 15 N, the drilling rate exhibited a significant decline.

Additionally, we observed that the free mass exhibited minimal oscillation at a WOB of 10 N and was seized at

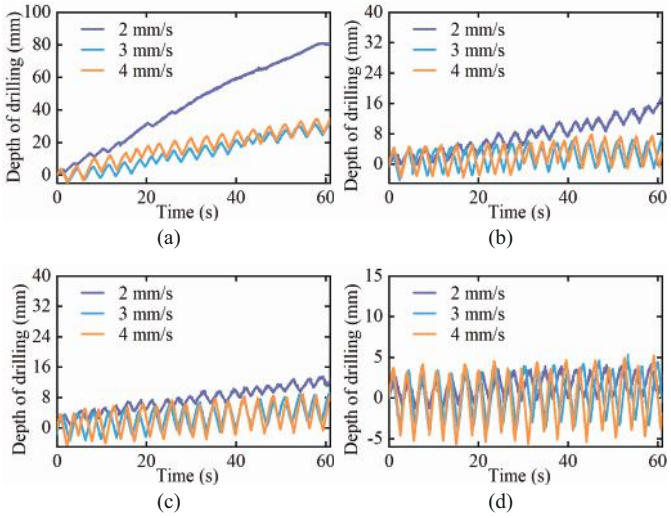

Fig. 8. Selection of response speed for linear actuator. (a) Aircrete. (b) Limestone. (c) Sandstone. (d) Marble.

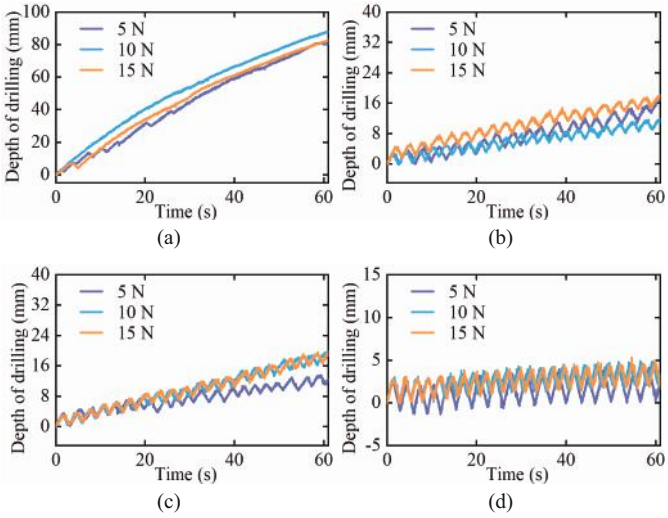

Fig. 10. Drilling depth with WOB active control. (a) Aircrete. (b) Limestone. (c) Sandstone. (d) Marble.

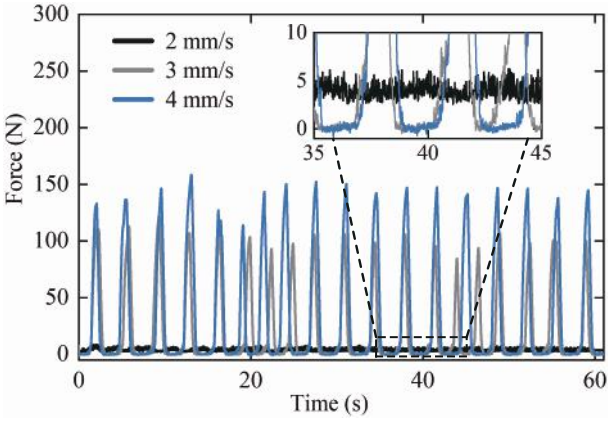

Fig. 9. Changes in WOB monitored by force sensing during active control while drilling aircrete.

a WOB of 15 N. Moreover, the oscillation amplitude of the free mass decreased as the rock's compressive strength increased. This reduction in free mass oscillation impacted the transmission of ultrasonic energy to the drill tool, resulting in a decreased drilling rate.

C. Response Speed of the Linear Actuator

Before conducting the active control test, the first step is to select the appropriate response speed for the linear actuator. The linear actuator offers a response speed range of 2 to 8 mm/s. Drawing from previous drilling rate studies, we selected three response speeds for testing: 2 mm/s, 3 mm/s, and 4 mm/s. The WOB was set at 5 N, and each drilling session lasted 1 minute. The power amplifier's output current was maintained at 0.6 A.

The test results are presented in Fig. 8. The UPD demonstrated stable drilling performance across all four types of rocks. If the UPD cannot break the rock faster than the linear actuator's forward movement at a response speed, the WOB detected by the force sensor exceeds 5 N. Consequently, the linear actuator moves backward alongside the UPD. In Fig. 8, the triangular-shaped curve represents the backward movement of the UPD. Notably, as the response speed increases, the backward movement of the linear actuator becomes more pronounced. Additionally, the backward movement of the linear actuator increases with higher rock compressive strength. This backward motion reduces the effective drilling time of the UPD, consequently diminishing the drilling speed. Therefore, a linear actuator response speed of 2 mm/s was selected.

Fig. 9 illustrates the variation in WOB corresponding to the three response speeds of the linear actuator during UPD drilling on aircrete. As shown in the figure, when the response speed is set to 2 mm/s, the WOB is predominantly maintained at 5 N, with minimal backward movement of the linear actuator. The drilling depth curve in Fig. 8(a) remains nearly linear. Conversely, at response speeds of 3 mm/s and 4 mm/s, the maximum detected WOB values reach 110 N and 160 N, respectively, with consistent backward movement of the linear actuator.

D. Drilling Tests of Active Control

After determining the response speed of the linear actuator, we conducted tests to evaluate the drilling performance of the UPD at WOB levels of 5 N, 10 N, and 15 N. All other parameter settings remained consistent with those outlined in subsection C.

The test results are presented in Fig. 10. In each set of tests, the UPD demonstrated stable drilling performance. When the UPD drilled into aircrete, minimal backward movement of the linear actuator was observed, resulting in drilling depths exceeding 80 mm within 1 minute. Additionally, drilling depth exhibited a slight increase with higher WOB levels. However, when drilling into the other three rock types, the linear actuator exhibited backward movement.

For sandstone and marble, drilling depths also increased slightly with higher WOB levels. In the case of limestone, the drilling depth at a WOB of 5 N was less than that at a WOB of 15 N but greater than that at a WOB of 10 N. In several tests,

TABLE III
COMPARISON OF DRILLING DEPTH AT ONE MINUTE BETWEEN PASSIVE AND ACTIVE CONTROL

		Passive control				Active control			
Output current	WOB	Aircrete	Limestone	Sandstone	Marble	Aircrete	Limestone	Sandstone	Marble
0.6 A	5 N	73.2 mm	24.8 mm	29.5 mm	3.20 mm	81.2 mm	15.5 mm	10.7 mm	1.82 mm
	10 N	18.3 mm	4.11 mm	11.6 mm	1.42 mm	83.4 mm	9.60 mm	17.2 mm	2.30 mm
	15 N	4.60 mm	0.62 mm	0.93 mm	0.21 mm	87.2 mm	16.5 mm	17.7 mm	2.51 mm
0.8 A	5 N	—	—	50.2 mm	9.42 mm	—	—	57.9 mm	6.30 mm
	10 N	—	—	56.5 mm	3.25 mm	—	—	49.2 mm	3.72 mm
	15 N	—	—	43.3 mm	0.91 mm	—	—	49.5 mm	3.95 mm

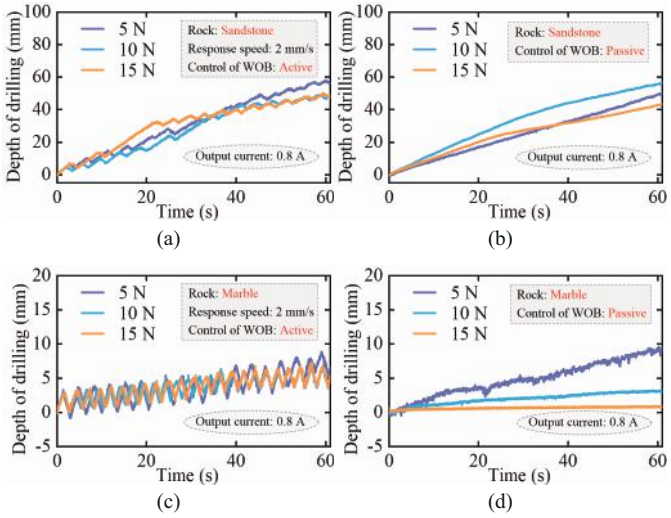

Fig. 11. Comparison of drilling depths at high amplitudes. (a) Active control of WOB during drilling in sandstone. (b) Passive control of WOB during drilling in sandstone. (c) Active control of WOB during drilling in marble. (d) Passive control of WOB during drilling in marble.

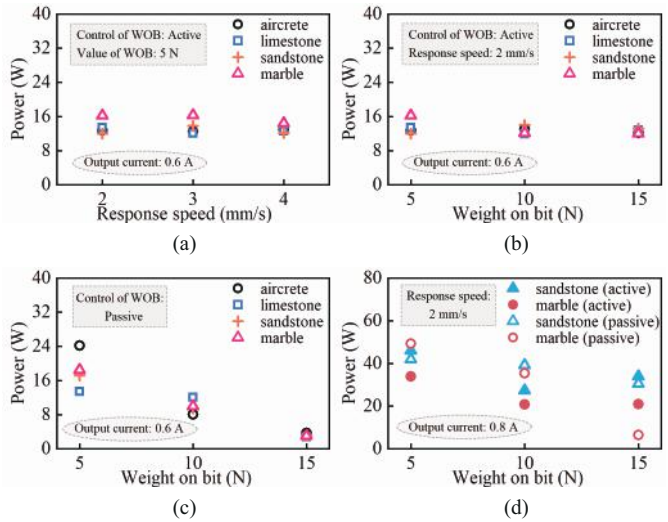

Fig. 12. Comparison of drilling active power consumption. (a) UPD Power consumption with active WOB control at different linear actuator response speeds. (b) UPD power consumption with active WOB control at different WOB levels. (c) UPD power consumption with passive WOB control at different WOB levels. (d) UPD power consumption with increased amplitude of piezoelectric transducer. Solid represents WOB active control, while hollow represents WOB passive control.

it was found that drilling depth did not increase with higher WOB levels when the UPD drilled into limestone, which might be caused by the higher cohesiveness of limestone.

E. Drilling at a High Amplitude

Through subsection D, we observed that for aircrete with low compressive strength, the UPD exhibited minimal backward movement during drilling. This observation suggests that an output current of 0.6 A is sufficient for the UPD to easily drill into aircrete. However, for rocks with higher compressive strength, an output current of 0.6 A does not achieve the desired fast drilling effect. Additionally, as noted in subsection B, increasing the WOB at an output current of 0.6 A reduces the oscillation of the free mass, subsequently decreasing the drilling rate. Therefore, in this subsection, we increased the output current to 0.8 A for the drilling tests.

Sandstone and marble were used for the study, because they are the more challenging materials. The variable parameters of the tests remained consistent with those in subsections B and D, respectively. The test results are presented in Fig. 11. As shown in Fig. 11(a), increasing the output current significantly reduced the backward movement of the linear actuator on sandstone. The drilling depth ranged from 49 to 58 mm, which is three times higher than that achieved with an output current of 0.6 A.

In Fig. 11(b), it is evident that the free mass exhibited normal oscillation when the WOB was set at 10 N and 15 N. At a WOB of 10 N, the drilling depth reached 56.5 mm, a fivefold improvement compared to the 0.6 A output current. When the WOB was increased to 15 N, the drilling depth reached 43.3 mm, a remarkable 47-fold improvement compared to the 0.6 A output current. Similarly, drilling depths on marble showed some improvement. However, when drilling passively into marble, the free mass still exhibited reduced oscillation at WOB levels of 10 N and 15 N, resulting in drilling depths of less than 3.2 mm in both cases. Thus, it can be concluded that increasing the output current is effective in reducing the backward motion of the linear actuator in active control and mitigating the adverse impact of excessive WOB on the free mass oscillation in passive control. This, in turn, leads to increased drilling depth. A comparison of drilling depths for passive and active control is provided in Table III.

F. Power and Energy Consumption

The power consumption (active power) of the UPD is obtained by calculating the voltage and current of the power amplifier output, which are captured by the Picoscope. The host computer performs real-time power calculations and displays the results. The power consumption of the UPD under both passive and active control is presented in Fig. 12.

Fig. 12(a) and Fig. 12(b) illustrate the power consumption of the piezoelectric transducer with an amplitude of 44.6 μm and active WOB control. Interestingly, different WOB levels and feed speeds have virtually no effect on power consumption. Similarly, the compressive strength of the rock exhibits minimal influence on power consumption. The overall power consumption values range from 12 to 17 W. Moreover, the effect of WOB, feed speed, and rock compressive strength on the power consumption of the linear actuator is negligible, with an average power consumption of 5 W.

Fig. 12(c), the power consumption of the piezoelectric transducer with an amplitude of 44.6 μm is depicted under passive WOB control. Here, we observe that power consumption decreases with increasing WOB, and the decrease is quite noticeable. Overall, power consumption values range from 4 to 26 W.

Fig. 12(d) demonstrates the power consumption of the UPD when the amplitude of the piezoelectric transducer is 58.2 μm. The trend in power consumption is similar to that observed with a 44.6 μm amplitude. As the amplitude of the piezoelectric transducer increases, the power of the UPD also increases. The maximum power consumption reaches 49 W.

V. Conclusion

To address the issue of weight-on-bit control of UPD on the surface of an asteroid, this paper firstly proposes the mechanical configuration of UPD that can adapt to the asteroid's environment and investigates the performance of the piezoelectric transducer through numerical simulation and experimental methods. Subsequently, two weight-on-bit control methods, passive control and active control, are introduced. Finally, the effects of these two weight-on-bit control methods on the drilling performance of the UPD are analysed through experimental comparisons. The following are some conclusions:

(1) The proposed UPD configuration is simple and easy to assemble. The validity of the numerical design method for the piezoelectric transducer is experimentally verified, with a difference of only 0.05% between the theoretical design frequency and the actual test frequency. The amplitude gain of the piezoelectric transducer can reach 10.15.

(2) When the amplitude of the piezoelectric transducer is small, the drilling rate decreases as WOB increases in passive control, while in active control, the drilling rate increases slightly with an increase in WOB. Passive control exhibits better drilling performance than active control when the WOB is 5 N; however, active control outperforms passive control when the WOB exceeds 5 N. After increasing the amplitude of the piezoelectric transducer, there is little difference between passive and active control for rocks with lower compressive strengths. For rocks with higher compressive strengths, the drilling performance pattern is similar to that when the amplitude is lower.

(3) When the WOB is 5 N, the power consumption of passive and active control is approximately the same. With passive control, power consumption decreases as WOB increases. With active control, power consumption is essentially independent of WOB and rock compressive strength. Overall, active control is better suited to variations in WOB and rock compressive strength, regardless of whether the piezoelectric transducer has high or low amplitude.

(4) During active-controlled drilling, a sharp increase in WOB leads to frequent backward movement of UPD, which reduces the effective drilling time. Meanwhile, the backward movement of the UPD facilitates the elimination of cuttings powder, which may be the reason for the difference between the two control methods. Further optimization of the control algorithm for the linear actuator needs to be explored in future research.

References

[1] E. Gibney, "Asteroids, hubble rival and moon base: China sets space plan," *Nature*, vol. 603, p. 19, 2022.

[2] T. Wang, Q. Quan *et al.*, "Progress in the development of small-celestial-body anchoring robots," *Nat. Astron.*, vol. 7, no. 4, pp. 380–390, 2023.

[3] Y. Bar-Cohen, S. Sherrit *et al.*, "Ultrasonic/sonic drilling/coring (usdc) for in-situ planetary applications," in *SPIE's 7th Annual International Symposium on Smart Structures and Materials*, Newport Beach, CA, USA, 2000, pp. 661–668.

[4] X. Li and D. J. Scheeres, "The shape and surface environment of 2016 ho3," *Icarus*, vol. 357, p. 114249, 2021.

[5] A. Allam, C. L. Arrington *et al.*, "System-level dc-to-dc analysis and experiments of ultrasonic power transfer through metallic barriers," *IEEE/ASME Trans. Mechatron.*, vol. 28, no. 1, pp. 15–25, 2022.

[6] Q. Zhang, D. Tang *et al.*, "Hill-climbing & fuzzy combined control algorithm for a percussive ultrasonic drill," *Appl. Acoust.*, vol. 211, p. 109499, 2023.

[7] J. Wu, J. Niu *et al.*, "Development of a self-moving ultrasonic actuator with high carrying/towing capability driven by longitudinal traveling wave," *IEEE/ASME Trans. Mechatron.*, vol. 28, no. 1, pp. 267–279, 2022.

[8] Q. Quan, T. Wang *et al.*, "An ultrasonic drilling system for fast drilling speed with uncertain load," *IEEE/ASME Trans. Mechatron.*, vol. 28, no. 3, pp. 1477–1487, 2022.

[9] Y. Bar-Cohen, Z. Chang, S. Sherrit *et al.*, "The ultrasonic/sonic driller/corer (usdc) as a subsurface drill, sampler, and lab-on-a-drill for planetary exploration applications," in *SPIE Smart Structures and Materials + Nondestructive Evaluation and Health Monitoring*, San Diego, CA, USA, 2005.

[10] Y. K. Yong, A. A. Eielsen, and A. J. Fleming, "Thermal protection of piezoelectric actuators using complex electrical power measurements and simplified thermal models," *IEEE/ASME Trans. Mechatron.*, early access, doi: 10.1109/TMECH.2023.3277437.

[11] S. Ye, Z. Long, J. Ju *et al.*, "Toward ultrasonic wire bonding for high power device: A vector based resonant frequency tracking and constant amplitude control," *IEEE Trans. Autom. Sci. Eng.*, vol. 20, no. 2, pp. 1337–1348, 2022.

[12] J. Gao and Y. Altintas, "Development of a three-degree-of-freedom ultrasonic vibration tool holder for milling and drilling," *IEEE/ASME Trans. Mechatron.*, vol. 24, no. 3, pp. 1238–1247, 2019.

[13] N. Guo, X. Luo *et al.*, "A novel mathematical method for calculating the lcl-type matching of ultrasonic transducer for liquefaction treatment," *IEEE Sensors Journal*, vol. 23, no. 8, pp. 8737–8743, 2022.

[14] X. Li, A. Meadows, V. Babitsky, and R. Parkin, "Experimental analysis on autoresonant control of ultrasonically assisted drilling," *Mechatronics*, vol. 29, pp. 57–66, 2015.

[15] X. Li, P. Harkness, K. Worrall *et al.*, "A parametric study for the design of an optimized ultrasonic percussive planetary drill tool," *IEEE Trans. Ultrason., Ferroelect., Freq. Control*, vol. 64, no. 3, pp. 577–589, 2016.

[16] S. Sherrit, L. Domm *et al.*, "Single piezo-actuator rotary-hammering (sparh) drill," in *Sensors and Smart Structures Technologies for Civil, Mechanical, and Aerospace Systems*, San Diego, CA, USA, 2012.

[17] X. Bao, Y. Bar-Cohen *et al.*, "Modeling and computer simulation of ultrasonic/sonic driller/corer (usdc)," *IEEE Trans. Ultrason., Ferroelect., Freq. Control*, vol. 50, no. 9, pp. 1147–1160, 2003.

[18] Y. Bar-Cohen, X. Bao *et al.*, "An ultrasonic sampler and sensor platform for in situ astrobiological exploration," in *Smart Structures and Materials 2003: Smart Structures and Integrated Systems*, San Diego, CA, USA, 2003, pp. 457–465.

[19] Y. Bar-Cohen, S. Sherrit *et al.*, "Subsurface ice and brine sampling using an ultrasonic/sonic gopher for life detection and characterization in the mcmurdo dry valleys," in *Smart Structures and Materials 2004: Industrial and Commercial Applications of Smart Structures Technologies*. SPIE, San Diego, CA, USA, 2004, pp. 53–61.

[20] M. Badescu, A. Ressa *et al.*, "Auto-gopher: a wireline deep sampler driven by piezoelectric percussive actuator and em rotary motor," in *Sensors and Smart Structures Technologies for Civil, Mechanical, and Aerospace Systems*, San Diego, CA, USA, 2013, pp. 782–789.

[21] P. Thomas, "Magna parva and esa's ultrasonic drill tool for planetary surface exploration," in *Earth and Space 2010: Engineering, Science, Construction, and Operations in Challenging Environments*, Hawaii, USA, 2010.

[22] J. Guo *et al.*, "A new ultrasonic / sonic drilling device," *Piezoelectric Acoustooptics*, vol. 30, no. 5, pp. 577–589, 2008.

[23] K. Zacny, G. Paulsen, Y. Bar-Cohen *et al.*, "Wireline deep drill for exploration of mars, europa, and enceladus," in *2013 IEEE aerospace conference*, Big Sky, MT, USA, 2013, pp. 1–14.

[24] Y. Bar-Cohen, S. Sherrit *et al.*, "Drilling, coring, and sampling using piezoelectric actuated mechanisms: From the usdc to a piezo-rotary-hammer drill," in *Earth and Space 2012: Engineering, Science, Construction, and Operations in Challenging Environments*, 2012.

[25] X. Bao, J. Scott, K. Boudreau *et al.*, "High temperature piezoelectric drill," in *Sensors and Smart Structures Technologies for Civil, Mechanical, and Aerospace Systems*, San Diego, CA, USA, 2009, pp, 783–790.

[26] V. N. Khmelev, V. A. Nesterov *et al.*, "The development of experimental sample of ultrasonic equipment for the intake of lunar soil," in *International Conference and Seminar of Young Specialists on Micro/Nanotechnologies and Electron Devices*, Altai, Russia, 2012, pp, 162–169.

[27] P. Harkness, M. Lucas, and A. Cardoni, "Architectures for ultrasonic planetary sample retrieval tools," *Ultrasonics*, vol. 51, no. 8, pp. 1026–1035, 2011.

[28] X. Li, M. Lucas, and P. Harkness, "Full and half-wavelength ultrasonic percussive drills," *IEEE Trans. Ultrason., Ferroelect., Freq. Control*, vol. 65, no. 11, pp. 2150–2159, 2018.

[29] X. Li and P. Harkness, "Autonomous and ultrasonically assisted drilling in a range of rocks and ice," *Ultrasonics*, vol. 125, p. 106803, 2022.

[30] D. Bai, Y. Li *et al.*, "Development of a rotary-percussive ultrasonic drill using a bolt-clamped type piezoelectric actuator," *Advances in Space Research*, vol. 71, no. 12, pp. 5360–5368, 2023.

[31] T. Wang, Q. Quan *et al.*, "An asteroid anchoring method based on cross-drilling geometric force closure of ultrasonic drill," *Acta Astronautica*, vol. 178, pp. 813–823, 2021.

[32] D. Bai, Q. Quan *et al.*, "Impact dynamics prediction of a rotary-percussive ultrasonic drill with a free mass," *IEEE Access*, vol. 6, pp. 32 649–32 661, 2018.

Tongzhao Wang was born in Anhui, China, in 1994. He received the bachelor's degree in mechanical design, manufacturing and automation from University of Science and Technology Liaoning, Anshan, China, in 2015, and the master's degree in mechanical engineering from Northeastern University, Shenyang, China, in 2018. He is currently pursuing the Ph.D. degree in mechanical engineering at Harbin Institute of Technology, Harbin, China.

His current research interest includes ultrasonic drive and control and asteroid anchoring and sampling.

Xuan Li was born in Beijing, China, in 1984. He is currently a research fellow at University of Glasgow, who is working on the Ultrasurge project-Innovative Miniature Ultrasonic Surgical Devices. He obtained his PhD in Mechanical and Manufacturing Engineering from Loughborough University in 2014, focused on resonance tracking system modelling and design of ultrasonic assisted drilling processes. He then worked as a research associate on the ultrasonic planetary core drill (UPCD) project for 3 years in the University of Glasgow. He had 1 year experience in designing miniature ultrasonic surgical device with Stryker Instruments. Prior to the start of the UltraSurge project in early 2019, he worked as a research engineer in the Advanced Manufacturing Research Centre (AMRC) at University of Sheffield for more than 1 year, focused on high power laser and ultrasonic assisted machining of aero-engine materials. His main research interests are high power ultrasonic applications.

Qiquan Quan (Senior Member, IEEE) was born in Anhui, China, in 1983. He received the bachelor degree in Automotive Engineering in 2005, master degree in Mechanical Design Theory in 2007 both at Harbin Institute of Technology, Harbin, China, and the Ph.D. in Robotics at Ritsumeikan University, Japan, in 2010.

He is holding a position of Professor in Faculty of Manufacture Engineering of Aerospace Vehicle at Harbin Institute of Technology. His current research interest includes Asteroid Anchoring and Sampling, Extraterrestrial Aerial Vehicle, Ultrasonic Drive and Control, Precise Torque Simulating and Testing.

Patrick Harkness was born in Dungannon, Norther Ireland, in 1980. He received the M.Eng. degree in aeronautical engineering from The Queen's University of Belfast, Belfast, U.K., in 2003, and the Ph.D. degree in space debris mitigation from Cranfield University, Cranfield, U.K., in 2007.

He is currently a Professor with the University of Glasgow, Glasgow, U.K. Prof. Harkness is a Fellow of the Institution of Mechanical Engineers. His research interests include sample acquisition on planetary surfaces and deployable structures in space.

Zongquan Deng was born in Heilongjiang, China, in 1956. He received his bachelor's degree and master's degree in mechanical design and theory from Harbin Institute of Technology, Harbin, China, in 1982 and 1984, respectively.

He is currently a Professor at the State Key Laboratory of Robotics and System at the Harbin Institute of Technology. His current research interests include special robot systems and aerospace mechanisms and control. Now, He is an academician of the Chinese Academy of Engineering.